Supplementary Information

Highly thermally conductive flame retardant epoxy nanocomposites with multifunctional ionic liquid flame retardant-functionalized boron nitride nanosheets

Xiongwei Li,[a] Yuezhan Feng,[a, b] Chao Chen,[c] Yunsheng Ye,[a*] Hongxia Zeng,[a] Hao Qu,[a] Jingwei Liu,[a] Xingping Zhou,[a] Shijun Long,[d] and Xiaolin Xie[a*]

[a]*Key laboratory of Material Chemistry for Energy Conversion and Storage, Ministry of Education, School of Chemistry and Chemical Engineering, Huazhong University of Science and Technology, Wuhan 430074, China.*

[b]*National Engineering Research Center for Advanced polymer Processing Technology, Zhengzhou University, Zhengzhou, 450002, China.*

[c]*Ministry-of-Education Key Laboratory for the Green Preparation and Application of Functional Materials, Faculty of Materials Science and Engineering, Hubei University, Wuhan 430062, China.*

[d]*School of Materials and Chemical Engineering, Hubei University of Technology, Wuhan 430068, China.*

Outline:

Table S2. Comparison of TC and TCE per 1 vol% values of our EP/ILFR-fBNNS composite with other polymer composites containing h-BN and BNNS.

References

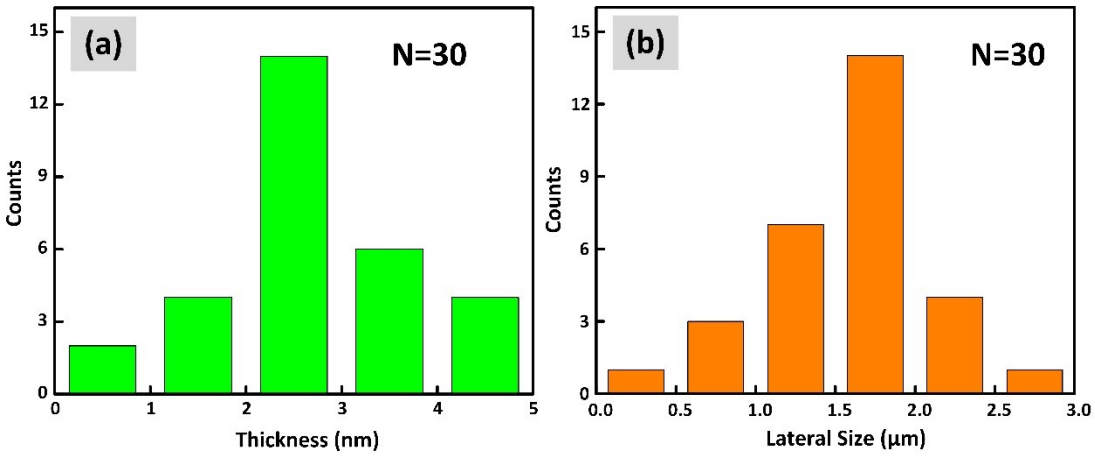

Figure S1. (a) Thickness and (b) lateral size histograms of ILFR-fBNNSs (30 flakes were measured by AFM).

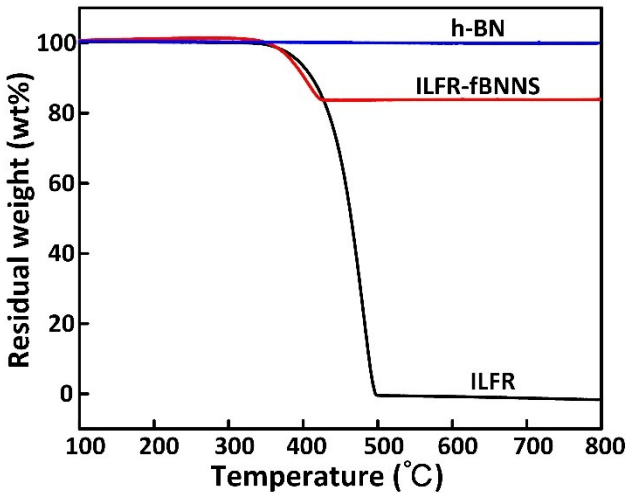

Figure S2. TGA curves of h-BN, ILFR and ILFR-fBNNS under a nitrogen atmosphere at a heating rate of 10 °C/min.

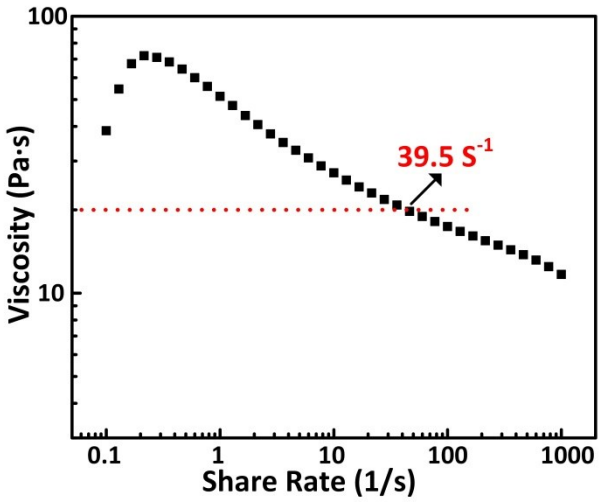

Figure S3. Steady shear viscosity of EP/ILFR-fBNNS suspension with a 12.1 vol% filler loading.

Curing mechanism of EP cross-linking with [BMIM]PF_6

The detailed curing processes of EP/[BMIM]PF_6/BDA can be summarized as follows (Figure S4a, 4b) according to previously related studies.[s1, s2] It's worth noting that PF_5 (as a Lewis acid) may have an accelerating effect on the EP cross-linking reaction. DSC results (Figure S4c) confirmed that the cross-linking reaction was mainly initiated by [BMIM]PF_6 rather than BDA, as the exothermic peak of EP/BDA was negligible.

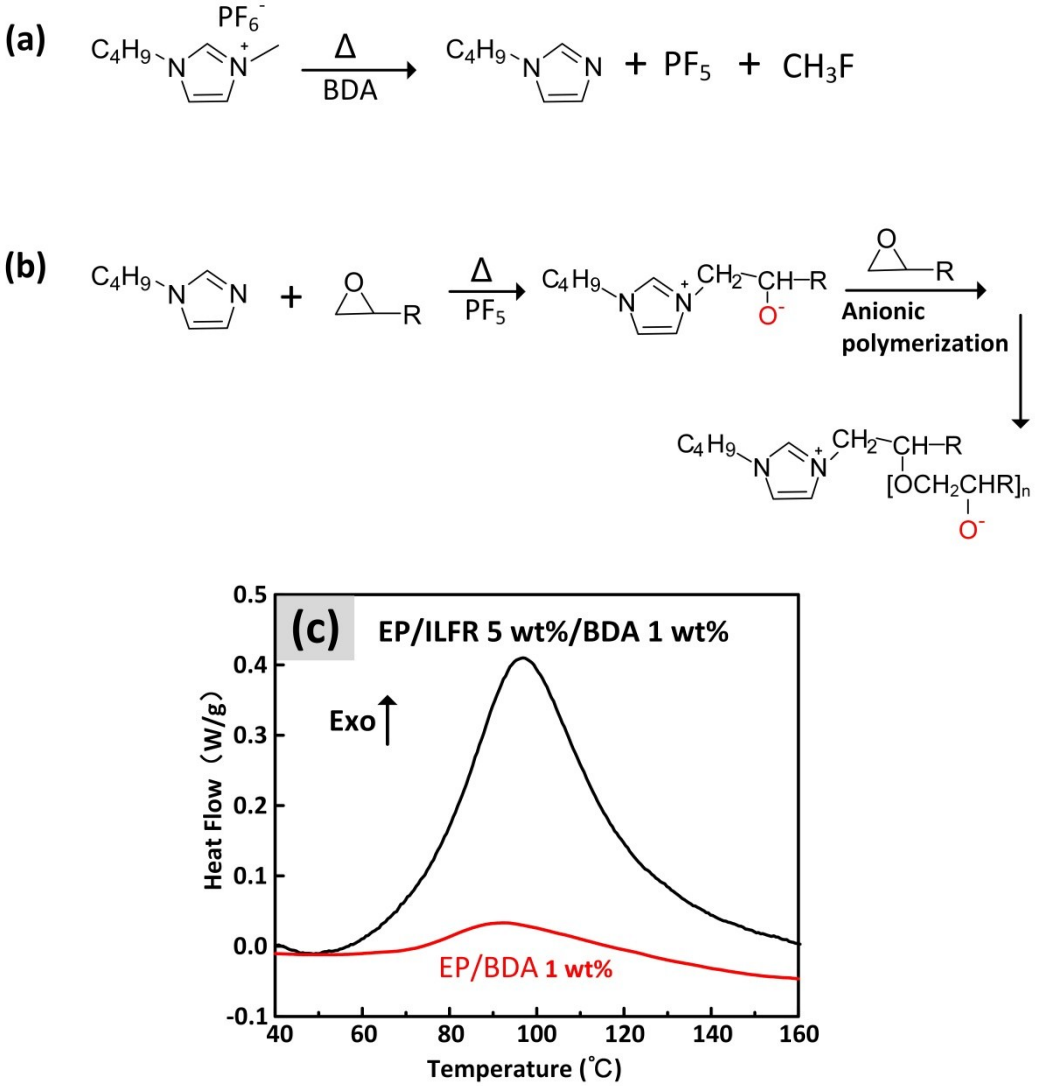

Figure S4. Proposed mechanism of EP cross-linking with [BMIM]PF_6. (a) decomposition of [BMIM]PF_6 into 1-butyllimidazoles, (b) 1-butylimidazole/EP 1:1 adduct formation and EP anionic polymerization and (c) DSC traces of EP/ILFR 5 wt%/BDA 1 wt% and EP/BDA 1 wt%.

The dispersion and morphology of BNNS in EP/ILFR-fBNNS nanocomposites were further investigated by FTEM. As shown in Figure S5a, BNNSs were finely dispersed in the EP matrix. The high resolution TEM (HRTEM) image and the fast FFT transform image (Figure S5b) also confirmed BNNSs remained few-layered and ordered structure without aggregation after curing process. In addition, the HRTEM images (Figure. S5c, 5d) at the edges of BNNSs clearly showed six to nine parallel fringes, indicating the BNNSs in the EP/ILFR-fBNNS nanocomposite mainly consisted of six to nine monolayers.

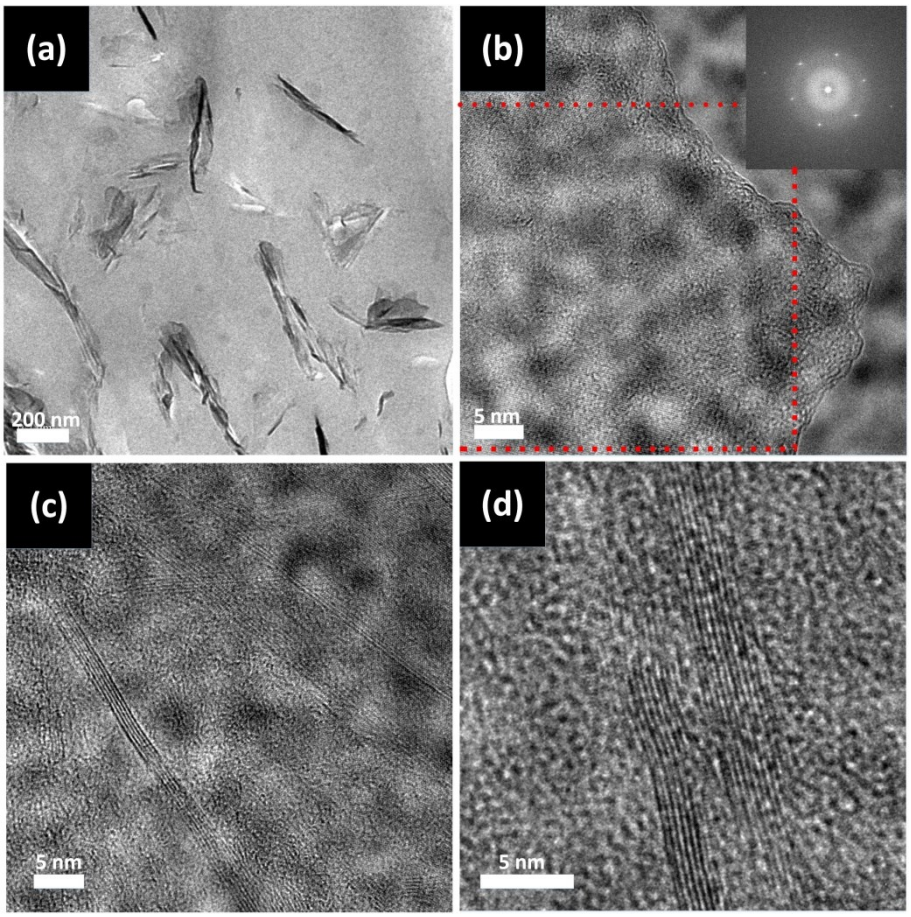

Figure S5. FTEM image of the fracture surface of EP/ILFR-fBNNS nanocomposites with a 12.1 vol% filler loading，inset in Figure S5b is the corresponding FFT pattern.

Effective medium approximation for the calculation of interfacial thermal resistance (ITR) of composite

To analyze our experimental results, we used the Maxwell-Garnett effective medium approximation (EMA) to calculate ITR (R_b), which gives the TC of the composite as:

$$K^*_{11} = K^*_{22} = K_m \frac{2 + f[\beta_{11}(1 - L_{11})(1 + \langle cos^2\phi\rangle) + \beta_{33}(1 - L_{33})(1 - \langle cos^2\phi\rangle)]}{2 - f[\beta_{11}L_{11}(1 + \langle cos^2\phi\rangle) + \beta_{33}L_{33}(1 - \langle cos^2\phi\rangle)]},$$

$$K^*_{33} = K_m \frac{1 + f[\beta_{11}(1 - L_{11})(1 + \langle cos^2\phi\rangle) + \beta_{33}(1 - L_{33})(1 - \langle cos^2\phi\rangle)]}{1 - f[\beta_{11}L_{11}(1 + \langle cos^2\phi\rangle) + \beta_{33}L_{33}(1 - \langle cos^2\phi\rangle)]},$$

with

$$\beta_{ii} = \frac{K^c_{ii} - K_m}{K_m + L_{ii}(K^c_{ii} - K_m)},$$

$$\langle cos^2\phi\rangle = \frac{\int \rho(\phi) cos^2\phi sin\phi d\phi}{\int \rho(\phi) sin\phi d\phi}.$$

Here ϕ is the angle between the material axis X_3 and the the normal of BNNS. ρ(φ) is the distribution function about particle orientation, f is the volume fraction, K_{ii}^c is the equivalent TC along symmetric axis of the composite unit cell.

$$K^c_{ii} = \frac{K_p}{1 + \frac{\gamma L_{ii} K_p}{K_m}},$$

where K_m and K_p are the TC of the matrix and filler; L_{ii} is the geometrical factor dependent on the shape of particle given by:

$$L_{11} = L_{22} = \frac{p^2}{2(p^2 - 1)} + \frac{p}{2(1 - p^2)^{\frac{3}{2}}} cos^{-1}p, \quad \text{for } p < 1,$$

$$L_{33} = 1 - 2L_{11}.$$

Where $p = a_3/a_1$ is the aspect ratio of filler (for platelets, $a_1 = a_2 > a_3$),

$$\gamma = (1 + 2p)\alpha, \text{ when } p < 1.$$

Here α is a dimensionless parameter about the interfacial properties between filler and matrix defined as:

$\alpha = \frac{R_b K_m}{a_3}$, with $R_b = \lim\left(\frac{\delta}{K_s}\right), \delta, K_s \to 0$, assuming interface layer with a thickness of δ and TC of K_s.

For randomly oriented BNNS, $\langle cos^2\phi\rangle = 1/3$, thus K^*_{33} could be:

$$K^*_{33} = K_m \frac{3 + f[2\beta_{11}(1 - L_{11}) + \beta_{33}(1 - L_{33})]}{3 - f[2\beta_{11}L_{11} + \beta_{33}L_{33}]}.$$

For the extraction of R_b, the theoretical TC of BNNS and the measured TC of neat EP are input as known parameter:

$K_m = 0.18\ W\ m^{-1}K^{-1}$, $K_p = 360\ W\ m^{-1}K^{-1}$.

The aspect ratio (p) of BNNS is estimated as: $p = 0.002$ according to our AFM statistic results.

Then, the data fitting results for EP/BNNS and EP/ILFR-fBNNS nanocomposites are show in Figure S5.

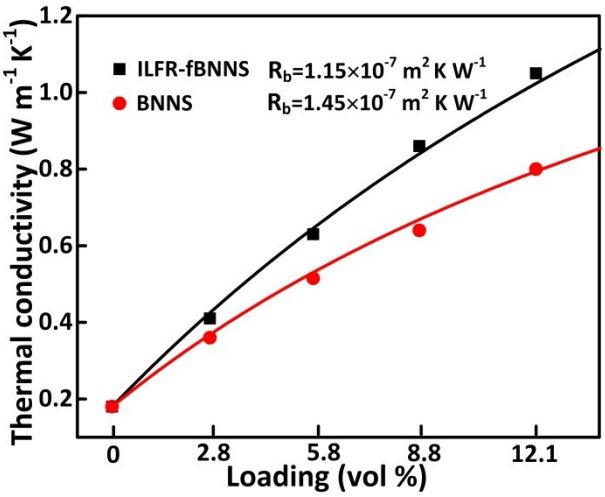

Figure S6. The model fitting curves and the corresponding thermal conductivity data of EP/BNNS and EP/ILFR-fBNNS (dots are the experimental data and lines are the fitting curves of EMA models).

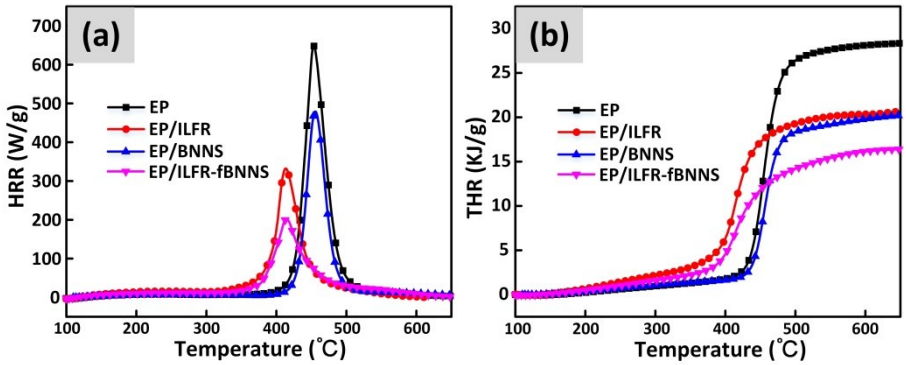

Figure S7. (a) Heat release rate, (b) total heat release curves of neat EP, EP/ILFR, EP/BNNS 12.1 vol% and EP/ILFR-fBNNS 12.1 vol% samples obtained from MCC.

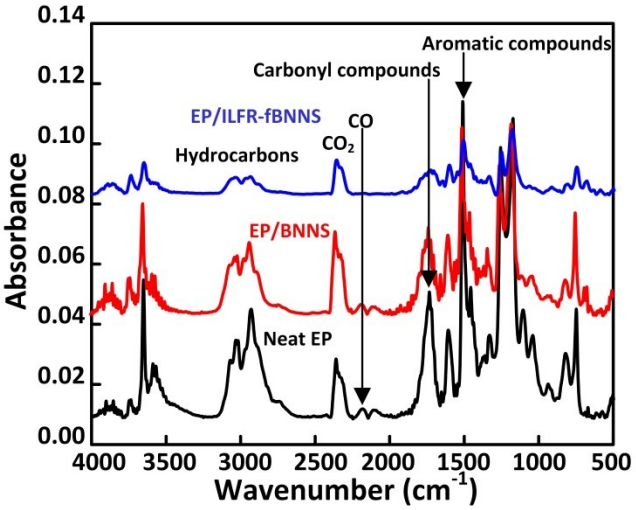

Figure S8. FTIR spectra of pyrolysis gaseous products emitted from neat EP, EP/BNNS and EP/ILFR-fBNNS at the maximum degradation rate.

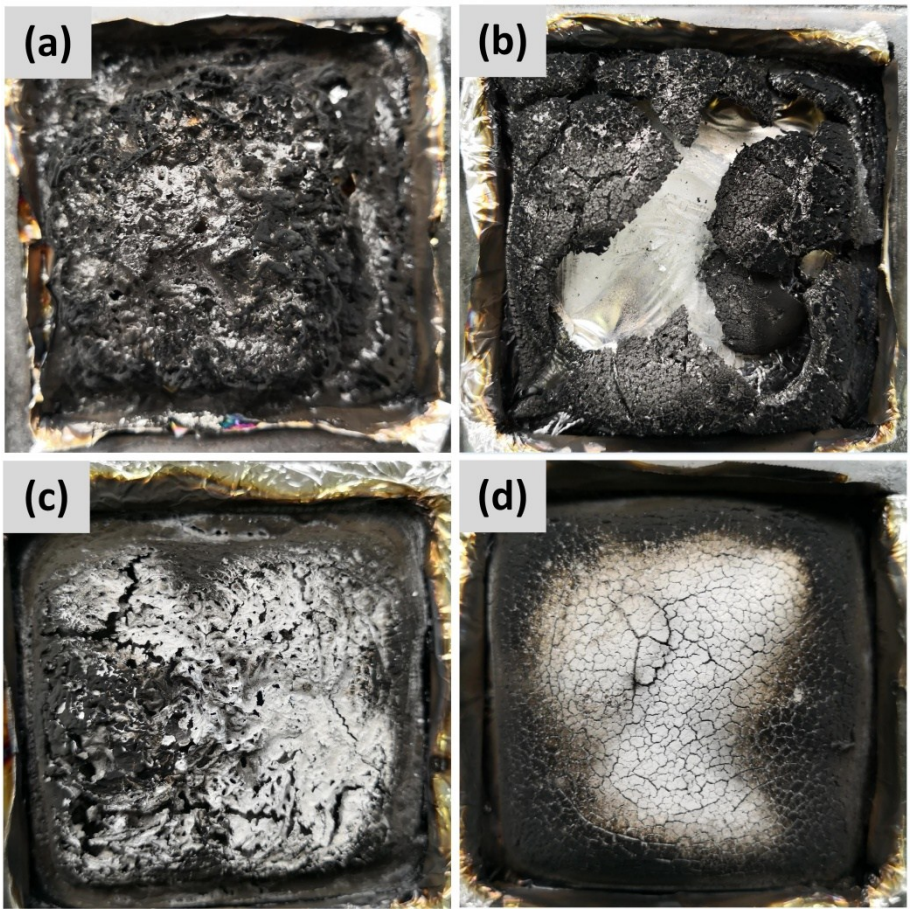

Figure S9. Digital photos of the residues after cone calorimeter test of (a) neat EP, (b) EP/ILFR, (c) EP/BNNS 12.1 vol%, (d) EP/ILFR-fBNNS 12.1 vol%.

Based on the previous studies,[s3, s4] the formation of a thermosetting network structure in this system is probably dependent on two reactions: the adduct reaction of epoxide groups with ILFR and subsequent etherification of hydroxyl groups. Thus, insufficient ILFR is not enough for efficient EP curing, and excess ILFR results in a large number of initiating species formed at the expense of ether linkages, both of which will reduce the crosslinking density, thereby reducing the mechanical and thermal properties. To obtain a mechanically and thermally strong EP matrix, which strongly depends on the composition ratio of the EP/ILFR, we have prepared EP thermosets with range concentrations of ILFR as curing agents and examined the glass transition temperature (T_g) and tensile mechanical properties of these thermosets. The experimental results are given in Table S1. Based on these physical properties, the amount of ILFR was optimized to be 5 wt% with respect to EP to achieve the best thermal and mechanical performances. Also, we have prepared EP/EMI-2,4 for comparison. It can be seen that EP/5 wt% ILFR has similar tensile strength compared with epoxy resin/EMI-2,4, which indicates the two systems have similar crosslinking densities; however, the T_g of EP/5 wt% ILFR (125.1 ^{o}C) is lower than that of EP/EMI-2,4 (133.8 ^{o}C), indicating there are still existing a few ILFR that are not crosslinked into the thermosetting network, which can increase the free volume of EP, thus leading to a reduced T_g.[s5]

Table S1. The tensile mechanical and glass transition of properties of neat EP (EP/EMI-2,4) and EP thermosets using various amounts of [BMIM]PF_6.

wt% of [BMIM]PF_6 relevant to epoxy	Tensile Strength (Mpa)	Tensile strain (%)	T_g (DSC)
3	64.74±1	4.46	121.2
5	68.29±2	4.39	125.1
7	63.73±2	4.95	123.7
9	61.40±4	4.52	122.3
EP/EMI-2,4	68.30±3	4.73	133.8

Table S2. Comparison of thermal conductivity and TCE per 1 vol% values of our EP/ILFR-fBNNS composite with other polymer composites containing h-BN and BNNS.

Filler	Composites	Loading (vol%)	K ($W\ m^{-1}\ K^{-1}$)	η (%)	References and year
h-BN	BECy/h-BN	15.0	0.55	6.9	2015[s6]
	BD/CPh-BN	13.7	1.12	13.1	2014[s7]
	LCEP/h-BN	35.0	2.5	15.9	2013[s8]
	PTFE/h-BN	30.0	0.72	5.5	2017[9]
	PE/h-BN	29.7	2.60	14.1	2015[s10]
BNNS	PMMA/BNNS	14.2	0.96	23.6	2016[s11]
	PDMS/BNNS	4.7	0.56	15.2	2017[s12]
	EP/NDEBN	17.6	0.54	11.9	2017[s13]
	EP/BNNS	18.3	0.62	17.3	2014[s14]
oriented h-BN or BNNS	Silicone/h-BN	9.7	0.58	28.7	2015[s15]
	EP/h-BN	50.0	3.59	35.6	2016[s16]
	EP/h-BN	11.7	0.85	40.0	2013[s17]
	Silicone rubber/BNNS	30.8	2.08	45.0	2015[s18]
ILFR-fBNNS	EP/ILFR-fBNNS	12.1	1.04	39.5	This work

Note: BECy: Bisphenol E cyanate ester; BD: o, o'-diallylbisphenol A modified bismaleimide resin; CPh-BN: cyclophosphazene hybridized hBN; LCEP: Liquid crystalline epoxy resin; NDEBN: nanodiamond-attached exfoliated hexagonal BN nanoplates.

References

s1. M. C. Kroon, W. Buijs, C. J. Peters and G.-J. Witkamp, *Thermochim. Acta*, 2007, **465**, 40-47.

s2. H. Maka, T. Spychaj and R. Pilawka, *Ind. Eng. Chem. Res.*, 2012, **51**, 5197-5206.

s3. J. Galy, A. Sabra and J. Pascault, *Polym. Eng. Sci.*,1986, **26**, 1514-1523.

s4. M. A. M. Rahmathullah, A. Jeyarajasingam, B. Merritt, M. VanLandingham, S. H. McKnight and G. R. Palmese, *Macromolecules*, 2009, **42**, 3219-3221.

s5. N. Shirshova, A. Bismarck and S. Carreyette, *J. Mater. Chem. A*, 2013, **1**, 15300-15309.

s6. H. Wu and M. R. Kessler, *ACS Appl. Mater. Interfaces*, 2015, **7**, 5915-5926.

s7. W. Jin, L. Yuan, G. Liang and A. Gu, *ACS Appl. Mater. Interfaces*, 2014, **6**, 14931-14944.

s8. M. Harada, N. Hamaura, M. Ochi and Y. Agari, *Composites, Part B*, 2013, **55**, 306-313.

s9. C. Pan, K. Kou, Q. Jia, Y. Zhang, G. Wu and T. Ji, *Composites, Part B*, 2017, **111**, 83-90.

s10. X. Zhang, H. Wu and S. Guo, *Polym-plast Technol*, 2015, **54**, 1097-1105.

s11. T. Morishita and H. Okamoto, *ACS Appl. Mater. Interfaces*, 2016, **8**, 27064-27073.

s12. H. Fang, S.-L. Bai and C. P. Wong, *Composites, Part A*, 2017, **100**, 71-80.

s13. Y. Zhang, J. R. Choi and S.-J. Park, *Composites, Part A*, 2017, **101**, 227-236.

s14. Z. Lin, A. McNamara, Y. Liu, K.-S. Moon and C. P. Wong, *Compos. Sci. Technol*, 2014, **90**, 123-128.

s15. C. Yuan, B. Duan, L. Li, B. Xie, M. Huang and X. Luo, *ACS Appl. Mater. Interfaces*, 2015, **7**, 13000-13006.

s16. S. Xu, H. Liu, Q. Li, Q. Mu and H. Wen, *J. Mater. Chem. C*, 2016, **4**, 872-878.

s17. Z. Lin, Y. Liu, S. Raghavan, K. S. Moon, S. K. Sitaraman and C. P. Wong, *ACS Appl. Mater. Interfaces*, 2013, **5**, 7633-7640.

s18. Z. Kuang, Y. Chen, Y. Lu, L. Liu, S. Hu, S. Wen, Y. Mao and L. Zhang, *Small*, 2015, **11**, 1655-1659.